

First-principle solubilities of alkali and alkaline earth metals in Mg-B alloys

Roman V. Chepulsii and Stefano Curtarolo

*Department of Mechanical Engineering and Materials Science,
and Center for Theoretical and Mathematical Sciences,
Duke University, Durham, North Carolina 27708, USA*

(Dated: February 3, 2022)

By devising a novel framework, we present a comprehensive theoretical study of solubilities of alkali (Li, Na, K, Rb, Cs) and alkaline earth (Be, Ca, Sr, Ba) metals in the boron-rich Mg-B system. The study is based on first-principle calculations of solutes formation energies in MgB₂, MgB₄, MgB₇ alloys and subsequent statistical-thermodynamical evaluation of solubilities. The advantage of the approach consists in considering all the known phase boundaries in the ternary phase diagram. Substitutional Na, Ca, and Li demonstrate the largest solubilities, and Na has the highest (0.5-1 % in MgB₇ at $T = 650 - 1000$ K). All the considered interstitials have negligible solubilities. The solubility of Be in MgB₇ can not be determined because the corresponding low-solubility formation energy is negative indicating the existence of an unknown ternary ground state. We have performed a high-throughput search of ground states in binary Mg-B, Mg-A, and B-A systems, and we construct the ternary phase diagrams of Mg-B-A alloys based on the stable binary phases. Despite its high temperature observations, we find that Sr₉Mg₃₈ is not a low-temperature equilibrium structure. We also determine two new possible ground states CaB₄ and RbB₄, not yet observed experimentally.

PACS numbers: 74.70.Ad, 61.50.Ks, 81.30.Hd

I. INTRODUCTION

The interest in magnesium diboride emerged after the discovery of superconductivity in MgB₂ at about $T_c=39$ K.¹ Attempts to increase T_c by small additions of alkali (Li^{2,3,4,5,6}, Na^{7,8}, Rb^{9,10}, Cs^{9,10}) and alkaline earth (Be¹¹, Ca^{4,7,12,13}, Ba⁹) metals to MgB₂, proved to be unsuccessful. The difficulty was attributed not only to the inability of such solutes to decrease T_c but also to their low solubility and precipitation in secondary phases. Although a claimed superconductivity at 50K was reported for the Mg-B-A ($A=Cs, Rb, Ba$) system⁹, attempts to reproduce the results have been so far unsuccessful (for $A=Cs, Rb$)¹⁰. The problem can be attributed to solutes' segregation in grain boundaries and to thus to low solubility in the bulk phase (much lower than reported in Ref. 9).

For consistent interpretation of experimental observations, theoretical studies of solubility in Mg-B of alkali metals and alkaline earth metal solubilities are therefore necessary. For instance, in Ref. 14, the semi-empirical Miedema approach¹⁵ and the Toop's model¹⁶ were used to address the heats of formation of binary alloys Mg-A, B-A, and Mg-B ($A=Li, Na, and Ca$). It was proposed that Ca may form stable compounds while Na, Li could lead to meta-stable or unstable ternary phases in MgB₂. In Ref. 17, by calculating first-principle formation energies of Li and Na impurities in MgB₂, and by neglecting the effects of other ground states in the ternary phase diagram solubility calculations, it was concluded that Na should have very low solubility, whereas the solubility of Li should be comparatively higher although modestly

diminished by a segregation into LiB phase.

The present paper is orthogonal to previous studied. We develop a comprehensive theoretical framework to determine the solubilities of alkali metals (Li, Na, K, Rb, Cs) and alkaline earths (Be, Ca, Sr, Ba) in the boron-rich Mg-B system. The study consists of first-principle calculations of solutes formation energies in MgB₂, MgB₄, MgB₇ alloys and subsequent statistical-thermodynamical evaluation of solubilities with respect to *all known equilibrium states* of the Mg-B-A system. The results help outlining future directions in experimental searches.

The paper is organized as following. In Section II, we describe the adopted solubility mechanisms in Mg-B. In Section III, we introduce the relevant impurity formation energies in terms of supercell energy calculations and the appropriate ground state(s). In Section IV, the approximation for the free energy of Mg-B-A solid solution is formulated. In Section V, we present an approach for solubility calculation considering all the ternary ground states. A simple analytical low-solubility approximation is devised. Section VI is devoted to the high-throughput *ab initio* search for ground states in binary Mg-B, Mg-A, and B-A systems, to the ternary phase diagrams of Mg-B-A systems, and to the impurity formation energies determined through the phase boundaries of the systems. The numerical values of solubilities are presented in Section VII. Section VIII summarizes the results, draws conclusions, and comments on strategies for future research in this area.

II. MG-B-A SOLID SOLUTION

For the description of solubility of alkali and alkaline earth metal elements A ($A=\text{Li, Be, Na, Mg, K, Ca, Rb, Sr, Cs, Ba}$) in the Mg-B system, we consider the disordered solid solutions of A -atoms as interstitial and magnesium-substitutional impurities in the experimentally reported compounds^{18,19} MgB_2 , MgB_4 , and MgB_7 . We do not consider boron substitutions by A because they have not been observed experimentally^{2,3,4,5,6,7,8,9,10,11,12,13}. The disordered solid solution of A inside Mg-B is labeled as “(1)” throughout the paper.

While the magnesium-substitutional positions are determined¹⁹, the “most accommodating” interstitial locations have to be found. The task is implemented with the following exhaustive search performed through our software AFLOW^{20,21}. Let us consider a quadruplet of no-coplanar atoms, where the first atom belongs to the unit cell and the others are closer than the maximum diagonal of the unit cell to the first atom. A *cage* is defined when the spherical region of space touching all the four atoms of the quadruplet does not contain further atoms inside. An *interstitial* position is found if the cage has its center inside the unit cell. By considering all the possible combinations, the symmetrically inequivalent interstitials can be identified through the calculation of their site symmetry (with the factor group of the unit cell). Note that in unit cells with complex arrangements, many of the interstitials positions can be extremely close. Thus, an interstitial atom located in any of those close positions would deform the nearby local atomic environment and *relax* to the same final location. Hence, the number of symmetrically inequivalent cages can be further reduced by considering the whole set of positions that would *agglomerate* upon insertion of an interstitial atom, as a single interstitial position. The results of the search are presented in Table I. The table demonstrates that the higher boron contents the larger number of cages and the larger radius of the bigger cage.

III. FORMATION ENERGIES DEFINITIONS

“Raw” formation energies

Let us define the so-called “raw” formation energies μ_i and $\bar{\mu}_s$ (composition unpreserving²²) as the changes of the energies of the solvent upon introduction of one solute atom A in the i -th type interstitial or s -th type substitutional positions. In first-principles calculations, the solvent can be replaced by a large supercell (“ sc ”),

TABLE I: Centers and sizes of the symmetrically inequivalent interstitial cages for the MgB_2 , MgB_4 , and MgB_7 unit cells. Coordinates are presented as fractions of the standard unit cell basis vectors (a, b, c) ¹⁹. The radius is the distance from the cage center to the nearest Mg or B atom. ν_i indicates the numbers of the symmetrically equivalent cages within the unit cell. The total numbers of distinct geometrical cages before agglomeration upon insertion of an interstitial is reported in brackets.

Structure	i	Coordinates (fract. of a, b, c)	Cage radius (\AA)	ν_i
MgB_2	1	0.341, 0.681, 0.000	1.7619	2 (6)
	2	0.006, 0.000, 0.500	1.7616	1 (6)
	3	0.500, 0.500, 0.122	1.6015	6 (6)
MgB_4 (Mg_4B_{16})	1	0.106, 0.669, 0.412	1.9145	4 (52)
	2	0.375, 0.250, 0.337	1.7836	4 (4)
	3	0.145, 0.632, 0.813	1.7821	8 (24)
	4	0.144, 0.750, 0.925	1.7252	4 (24)
	5	0.225, 0.750, 0.719	1.6322	4 (4)
	6	0.086, 0.015, 0.527	1.6128	8 (8)
	7	0.101, 0.543, 0.261	1.5322	8 (8)
MgB_7 (Mg_8B_{56})	1	0.000, 0.049, 0.618	2.0050	8 (152)
	2	0.189, 0.250, 0.821	1.8937	8 (24)
	3	0.250, 0.217, 0.750	1.7995	8 (8)
	4	0.243, 0.250, 0.505	1.7888	8 (24)
	5	0.197, 0.250, 0.469	1.7802	8 (24)
	6	0.000, 0.250, 0.150	1.7002	4 (24)
	7	0.012, 0.000, 0.000	1.6995	8 (64)
	8	0.250, 0.062, 0.250	1.6068	8 (40)
	9	0.000, 0.171, 0.788	1.4991	8 (8)
	10	0.131, 0.186, 0.119	1.4443	16(16)

so that

$$\mu_i \equiv \mu_i^{(1)}(\text{A}) = E_{\text{SC}}[\text{A}^{(i)}\text{Mg}_{n_{\text{sc}}}\text{B}_{m_{\text{sc}}}] - E_{\text{SC}}[\text{Mg}_{n_{\text{sc}}}\text{B}_{m_{\text{sc}}}],$$

$$\bar{\mu}_s \equiv \mu_s^{(1)}(\text{A}) - \mu^{(1)}(\text{Mg}) = E_{\text{SC}}[\text{A}^{(s)}\text{Mg}_{n_{\text{sc}}-1}\text{B}_{m_{\text{sc}}}] - E_{\text{SC}}[\text{Mg}_{n_{\text{sc}}}\text{B}_{m_{\text{sc}}}], \quad (1)$$

where n_{sc} and m_{sc} are the numbers of Mg and B atoms in the supercell; $\mu^{(1)}(\text{Mg})$, $\mu_i^{(1)}(\text{A})$, and $\mu_s^{(1)}(\text{A})$ are the zero-temperature chemical potentials of the Mg-atom, and the A -atoms in the i -th interstitial and s -th substitutional positions, respectively²³.

The conventional unit cells of MgB_2 , MgB_4 , and MgB_7 are used to construct the appropriate supercells. The supercells are chosen to have solute-solute A - A distance at least ~ 2.5 times the nearest neighbor solvent bonds in order to diminish the contribution of the A - A interactions to the calculated energies. We use $2 \times 2 \times 2$ unit cells for MgB_2 , while there is no need to create supercells of MgB_4 and MgB_7 since their unit cells are already large enough. Note that boron-boron (B-B) bond is the shortest among the Mg-Mg, B-B, and Mg-B bonds. Table II summarizes the parameters of the supercells and Table III lists the supercell atomic compositions.

TABLE II: Numbers of atoms n, m (Mg_nB_m) in the conventional unit cells (“uc”) ¹⁹ and in the constructed supercells (“sc”) for MgB_2 , MgB_4 , and MgB_7 . ν_s indicates the number of symmetrically equivalent s -type Mg atom positions within the corresponding unit cell: $\sum_s \nu_s = n_{\text{uc}}$. d_{AA} and d_{BB} are the distances between the nearest solutes and nearest solvent atoms (boron-boron in our case) in the supercell.

Compound	n_{uc}	m_{uc}	ν_s	n_{sc}	m_{sc}	d_{BB} (Å)	$d_{\text{AA}}/d_{\text{BB}}$
MgB_2	1	2	1	8	16	1.7811	3.46
MgB_4	4	16	4	4	16	1.7004	2.60
MgB_7	8	56	4,4	8	56	1.7372	3.44

TABLE III: Interstitial and substitutional supercell atomic compositions ($x_{\text{A}}^{\text{sc}}, x_{\text{B}}^{\text{sc}}, x_{\text{Mg}}^{\text{sc}}$) as functions of the n_{sc} (for Mg) and m_{sc} (for B) numbers of atoms in the super cell.

	Interstitials	Substitutional
x_{A}^{sc}	$[1 + n_{\text{sc}} + m_{\text{sc}}]^{-1}$	$[n_{\text{sc}} + m_{\text{sc}}]^{-1}$
x_{B}^{sc}	$m_{\text{sc}}[1 + n_{\text{sc}} + m_{\text{sc}}]^{-1}$	$m_{\text{sc}}[n_{\text{sc}} + m_{\text{sc}}]^{-1}$
$x_{\text{Mg}}^{\text{sc}}$	$n_{\text{sc}}[1 + n_{\text{sc}} + m_{\text{sc}}]^{-1}$	$n_{\text{sc}}[n_{\text{sc}} + m_{\text{sc}}]^{-1}$

“True” formation energies

The “true” formation energies (composition preserving²²) are defined from the “raw” formation energies (composition unpreserving²²) as

$$\begin{aligned} E_{\text{A}}^{(i)} &\equiv \mu_i - \mu_{\text{A}}^{\text{pure}}, \\ E_{\text{A}}^{(s)} &\equiv \bar{\mu}_s + \mu_{\text{Mg}}^{\text{pure}} - \mu_{\text{A}}^{\text{pure}}, \end{aligned} \quad (2)$$

where $\mu_{\text{A}}^{\text{pure}}$ and $\mu_{\text{Mg}}^{\text{pure}}$ are the chemical potentials (energies per atom) of A - and Mg-atoms in pure A - and Mg-solids at zero temperature, respectively.

Low-solubility formation energies

In Ref. 24, a quantity called “low-solubility formation energy”, was shown to determine the dilute solubility in binary alloys through the temperature exponential factor. The quantity can be generalized to the case of Mg-B-A alloy as (compare with Eq. (29) in Ref. 24):

$$E_{\text{sol}}^{\alpha}(A) \equiv \Delta E_{\text{sc/at}}^{\alpha} / x_{\text{A}}^{\text{sc}} \quad (3)$$

with $\alpha = (i), (s)$ and

$$\begin{aligned} \Delta E_{\text{sc/at}}^{(i)} &= \frac{E_{\text{sc}}[A^{(i)}\text{Mg}_{n_{\text{sc}}}\text{B}_{m_{\text{sc}}}]}{1+n_{\text{sc}}+m_{\text{sc}}} - E_{\text{at}}^{\text{mix}}(x_{\text{A}}^{\text{sc}}, x_{\text{B}}^{\text{sc}}, x_{\text{Mg}}^{\text{sc}}), \\ \Delta E_{\text{sc/at}}^{(s)} &= \frac{E_{\text{sc}}[A^{(s)}\text{Mg}_{n_{\text{sc}}-1}\text{B}_{m_{\text{sc}}}]}{n_{\text{sc}}+m_{\text{sc}}} - E_{\text{at}}^{\text{mix}}(x_{\text{A}}^{\text{sc}}, x_{\text{B}}^{\text{sc}}, x_{\text{Mg}}^{\text{sc}}), \end{aligned} \quad (4)$$

where $E_{\text{at}}^{\text{mix}}(x_{\text{A}}^{\text{sc}}, x_{\text{B}}^{\text{sc}}, x_{\text{Mg}}^{\text{sc}})$ is the energy of a the three phase mixture at the same composition of the supercell (see Table III):

$$E_{\text{at}}^{\text{mix}}(x_{\text{A}}^{\text{sc}}, x_{\text{B}}^{\text{sc}}, x_{\text{Mg}}^{\text{sc}}) = X_1 \frac{E_{\text{uc}}[\text{Mg}_{n_{\text{uc}}}\text{B}_{m_{\text{uc}}}]}{n_{\text{uc}} + m_{\text{uc}}} + X_2 E_{\text{at}}^{(2)} + X_3 E_{\text{at}}^{(3)}. \quad (5)$$

The coefficients X_k ($k=1,2,3$) are determined from the following linear system of equations

$$\begin{cases} x_{\text{A}}^{\text{sc}} = X_2 x_{\text{A}}^{(2)} + X_3 x_{\text{A}}^{(3)} \\ x_{\text{B}}^{\text{sc}} = X_1 \frac{m_{\text{uc}}}{n_{\text{uc}}+m_{\text{uc}}} + X_2 x_{\text{B}}^{(2)} + X_3 x_{\text{B}}^{(3)} \\ x_{\text{Mg}}^{\text{sc}} = X_1 \frac{n_{\text{uc}}}{n_{\text{uc}}+m_{\text{uc}}} + X_2 x_{\text{Mg}}^{(2)} + X_3 x_{\text{Mg}}^{(3)}, \end{cases} \quad (6)$$

where $E_{\text{at}}^{(k)}, x_{\text{A}}^{(k)}, x_{\text{B}}^{(k)}, x_{\text{Mg}}^{(k)}$ ($k=2,3$) are the energies (per atom) and stoichiometric compositions of the two other ground states that, together with $\text{Mg}_{n_{\text{uc}}}\text{B}_{m_{\text{uc}}}$, form the *convex-hull triangle* containing the point $(x_{\text{A}}^{\text{sc}}, x_{\text{B}}^{\text{sc}}, x_{\text{Mg}}^{\text{sc}})$ in the ternary phase diagram. For example, MgB_2 , Mg, and LiB_3 are the three ground states surrounding $\text{Mg}_7\text{B}_{16}\text{Li}$ (a supercell of MgB_2 with a substitutional Li atom) as shown in Fig. 2. The coefficient X_k ($k=1,2,3$) represents the fraction of the k -th phase in the mixture. The quantities $\Delta E_{\text{sc/at}}^{\alpha}$ defined in Eq. (4) are the supercell formation energies (per atom) determined with respect to the mixture of ground states²⁴. $E_{\text{sol}}^{\alpha}(A)$ and $\Delta E_{\text{sc/at}}^{\alpha}$ can not be negative. If they do, it indicates that the list of ground states is incomplete, and a better phase diagram should be established (the missed ground state can be supercell itself)²⁴.

In analogy of with binary alloys²⁴, the ternary alloy “low-solubility formation energy” $E_{\text{sol}}^{\alpha}(A)$ is shown to determine the solubility of A in the low-solubility limit (Section V).

IV. FREE ENERGY OF MG-B-A SOLID SOLUTION

The Gibbs free energy per unit cell (“uc”) of the Mg-B-A solid solution is determined within the mean-field approximation:

$$G_{\text{uc}}^{(1)}[\{c_i, c_s\}, T] = E_{\text{uc}}[\text{Mg}_{n_{\text{uc}}}\text{B}_{m_{\text{uc}}}] + \Delta g_{\text{I}} + \Delta g_{\text{s}},$$

$$\begin{aligned} \Delta g_{\text{I}} &= \sum_i \nu_i \{c_i \mu_i + k_{\text{B}} T [c_i \ln c_i + (1 - c_i) \ln(1 - c_i)]\}, \\ \Delta g_{\text{s}} &= \sum_s \nu_s \{c_s \bar{\mu}_s + k_{\text{B}} T [c_s \ln c_s + (1 - c_s) \ln(1 - c_s)]\}, \end{aligned} \quad (7)$$

where k_{B} is a Boltzmann constant, T is the temperature, and $E_{\text{uc}}[\text{Mg}_{n_{\text{uc}}}\text{B}_{m_{\text{uc}}}]$ represents the energy (enthalpy) of initial $\text{Mg}_{n_{\text{uc}}}\text{B}_{m_{\text{uc}}}$ unit cell without A -solute; the summations over i and s are over all the inequivalent types of interstitial and substitutional positions in unit cell; c_i and c_s are equal to the *site*-concentrations of A -atoms at each

interstitial (*i*-) and substitutional (*s*-) type, respectively. Thus, we assume that the concentrations in the equivalent positions are equal in the disordered state. The “raw” formation energies μ_i and $\bar{\mu}_s$ are introduced in Sec. III. Although, the mean-field approximation neglects correlations, it should work well when the deviation from stoichiometry is small (see Sec. 19 in Ref. 25). In addition, we neglect solute-solute interactions that might be important especially for high solute concentrations. In conclusion, our model is similar to Wagner-Schottky model of a system of non-interacting particles²⁶.

For given concentrations $\{c_i, c_s\}$, the total number of atoms per unit cell, $N_{\text{uc}}^{\text{at}}$, the total concentrations of *A*-interstitials, $x_{\text{A}(i)}^{(1)}$, *A*-substitutional, $x_{\text{A}(s)}^{(1)}$, and the total concentration of *A*-atoms, $x_{\text{A}}^{(1)}$, are determined as

$$\begin{aligned} N_{\text{uc}}^{\text{at}} &= \sum_i \nu_i c_i + n_{\text{uc}} + m_{\text{uc}}, \\ x_{\text{A}(i)}^{(1)} &= \sum_i \nu_i c_i / N_{\text{uc}}^{\text{at}}, \quad x_{\text{A}(s)}^{(1)} = \sum_s \nu_s c_s / N_{\text{uc}}^{\text{at}}, \quad (8) \\ x_{\text{A}}^{(1)} &= x_{\text{A}(i)}^{(1)} + x_{\text{A}(s)}^{(1)}. \end{aligned}$$

At given temperature and concentration $x_{\text{A}}^{(1)}$, the Gibbs free energy per atom $G_{\text{at}}^{(1)}[x_{\text{A}}^{(1)}, T]$ is determined by minimizing Eq. (7) with respect to $\{c_i\}$ and $\{c_s\}$:

$$G_{\text{at}}^{(1)}[x_{\text{A}}^{(1)}, T] = \min_{\{c_i, c_s\}} \left[G_{\text{at}}^{(1)}[\{c_i, c_s\}, T] \right]_{x_{\text{A}}^{(1)}}, \quad (9)$$

where

$$G_{\text{at}}^{(1)}[\{c_i, c_s\}, T] = G_{\text{uc}}^{(1)}[\{c_i, c_s\}, T] / N_{\text{uc}}^{\text{at}}. \quad (10)$$

The solution $\{c_i, c_s\}$ defines the equilibrium distribution of interstitial and substitutional *A*-solute in the $\text{Mg}_{n_{\text{uc}}}\text{B}_{m_{\text{uc}}}$ solvent.

In the case of small concentrations of interstitials, the minimization can be done with the Lagrange multiplier method, obtaining:

$$c_i = \left[1 + \exp \frac{\mu_i + \mu(1 - x_{\text{A}}^{(1)})}{k_B T} \right]^{-1}, \quad c_s = \left[1 + \exp \frac{\mu_s + \mu}{k_B T} \right]^{-1}. \quad (11)$$

where the Lagrange multiplier μ is determined from the following equation (derived from Eq. (8)):

$$x_{\text{A}}^{(1)}(n_{\text{uc}} + m_{\text{uc}}) = \sum_i \nu_i c_i (1 - x_{\text{A}}^{(1)}) + \sum_s \nu_s c_s. \quad (12)$$

V. SOLUBILITY

According to Nernst’s theorem, either a single compound or a phase separation of compounds at correct stoichiometry can be present at equilibrium at zero temperature. At finite temperatures, the composition of phases

can differ from stoichiometry through solution because of the entropic promotion (Sec. VII and Ref. 24). At a given temperature, the solubility of *A*-atoms in a compound is defined as the maximum homogeneously achievable concentration of *A*-atoms, without the formation of a new phase.

To calculate the solubility²⁷, we consider the Gibbs free energy $G_{\text{at}}^{\text{mix}}$ of the mixture of three phases with a given general (“gen”) composition $x^{\text{gen}} \equiv (x_{\text{A}}^{\text{gen}}, x_{\text{B}}^{\text{gen}}, x_{\text{Mg}}^{\text{gen}})$. The first phase is the substitutional and/or interstitial solid solution with atomic concentration $x_{\text{A}}^{(1)}$ of element *A* in $\text{Mg}_{n_{\text{uc}}}\text{B}_{m_{\text{uc}}}$. At zero temperature, the two other phases and $\text{Mg}_{n_{\text{uc}}}\text{B}_{m_{\text{uc}}}$ form a triangle containing the point x^{gen} in the ternary phase diagram. At a finite temperature, the free energy $G_{\text{at}}^{\text{mix}}$ is the generalization of Eq. (5):

$$\begin{aligned} G_{\text{at}}^{\text{mix}}[x_{\text{A}}^{(1)}, T] &\simeq X_1[x_{\text{A}}^{(1)}, T]G_{\text{at}}^{(1)}[x_{\text{A}}^{(1)}, T] + \\ &X_2[x_{\text{A}}^{(1)}, T]E_{\text{at}}^{(2)} + X_3[x_{\text{A}}^{(1)}, T]E_{\text{at}}^{(3)}, \end{aligned} \quad (13)$$

where $G_{\text{at}}^{(1)}[x_{\text{A}}^{(1)}, T]$ is given by Eq. (9), and the second and third phases are assumed to be stoichiometric, so that their free energies can be approximated by their ground state energies (enthalpies) $E_{\text{at}}^{(2)}$ and $E_{\text{at}}^{(3)}$, respectively. The approximation does not affect much the results, as we are interested in the small solubility regime of *A*. Similarly to Eq. (6), the fractions X_k are determined by solving the system:

$$\begin{cases} x_{\text{A}}^{\text{gen}} = X_1 x_{\text{A}}^{(1)} + X_2 x_{\text{A}}^{(2)} + X_3 x_{\text{A}}^{(3)} \\ x_{\text{B}}^{\text{gen}} = X_1 x_{\text{B}}^{(1)} + X_2 x_{\text{B}}^{(2)} + X_3 x_{\text{B}}^{(3)} \\ x_{\text{Mg}}^{\text{gen}} = X_1 x_{\text{Mg}}^{(1)} + X_2 x_{\text{Mg}}^{(2)} + X_3 x_{\text{Mg}}^{(3)}, \end{cases} \quad (14)$$

where the second “(2)” and third “(3)” phases are at stoichiometry. In addition, we have

$$\begin{aligned} x_{\text{B}}^{(1)} &= \frac{n_{\text{uc}}}{n_{\text{uc}} + m_{\text{uc}}} \left(1 - x_{\text{A}(i)}^{(1)}[x_{\text{A}}^{(1)}, T] \right), \\ x_{\text{Mg}}^{(1)} &= 1 - x_{\text{A}}^{(1)} - x_{\text{B}}^{(1)}, \end{aligned} \quad (15)$$

where $x_{\text{A}(i)}^{(1)}[x_{\text{A}}^{(1)}, T]$ is the equilibrium concentration of *A*-interstitials in the first phase given by Eqs. (8-9) at for chosen total concentration $x_{\text{A}}^{(1)}$. The minimization of $G_{\text{at}}^{\text{mix}}$ with respect to $x_{\text{A}}^{(1)}$ gives the solubility $x_{\text{A}}^{(1)}(T)$ in the first phase “(1)”:

$$G_{\text{at}}^{\text{mix}}[x_{\text{A}}^{(1)}(T), T] = \min_{x_{\text{A}}^{(1)}} G_{\text{at}}^{\text{mix}}[x_{\text{A}}^{(1)}, T]. \quad (16)$$

This procedure, equivalent to the common-tangent method, is the generalization of the approach developed in Ref. 24 to the case of ternary alloys. The method is somehow different from that developed in Ref. 28. Although, the regular solution model used in Ref. 28 and

the presented ideal solution model coincide in the low solubility regime, the consideration of only two ground states (“*gs*”) by the authors of Ref. 28, differs from our approach requiring the knowledge of the whole ternary stability. This is because the disordered Mg-B-A solution does not generally belong to the Mg-B \leftrightarrow *gs*⁽²⁾ or Mg-B \leftrightarrow *gs*⁽³⁾ lines in the ternary phase diagram. Thus, we have to consider the phase mixture of Mg_{nuc}B_{muc}, *gs*⁽²⁾, and , *gs*⁽³⁾ to guarantee accurate estimation of the solubility.

Low-solubility approximation

In order to get the analytical expression for equilibrium solubilities from Eq. (16), further approximations are required: (a) the equilibrium concentration of solute *A* is small and (b) only substitutional or interstitial positions of one type α are occupied (this approximation will be **eliminated** at the end of section). Thus, from Eqs. (13,16)) we obtain:

$$\frac{\partial G_{\text{at}}^{\text{mix}}}{\partial x_{\text{A}}^{(1)}} \approx \frac{\partial E_{\text{at}}^{\text{mix}}}{\partial x_{\text{A}}^{(1)}} + X_1 \frac{\partial G_{\text{at}}^{(1)}[x_{\text{A}}^{(1)}, T]}{\partial x_{\text{A}}^{(1)}} = 0, \quad (17)$$

where

$$E_{\text{at}}^{\text{mix}}[x_{\text{A}}^{(1)}, x^{\text{gen}}] = X_1 E_{\text{at}}^{(1)} + X_2 E_{\text{at}}^{(2)} + X_3 E_{\text{at}}^{(3)}, \quad (18)$$

and the fractions $X_k = X_k[x_{\text{A}}^{(1)}, x^{\text{gen}}]$ come from Eqs. (14,15). Note that the *circa* (\approx) in Eq. (17) corresponds to approximation (a) applied to Eqs. (7,10):

$$\frac{\partial X_1}{\partial x_{\text{A}}^{(1)}} G_{\text{at}}^{(1)} \approx \frac{\partial X_1}{\partial x_{\text{A}}^{(1)}} E_{\text{at}}^{(1)}. \quad (19)$$

Equations (14,15) lead to:

$$\frac{\partial X_k}{\partial x_{\text{A}}^{(1)}} \approx -X_1 \frac{\partial X_k}{\partial x_{\text{A}}^{\text{gen}}} \quad (20)$$

and through Eq. (18):

$$\frac{\partial E_{\text{at}}^{\text{mix}}}{\partial x_{\text{A}}^{(1)}} \approx -X_1 \frac{\partial E_{\text{at}}^{\text{mix}}}{\partial x_{\text{A}}^{\text{gen}}}. \quad (21)$$

By using the expression of $G^{(1)}$ from Eq. (7), we have

$$\frac{\partial G_{\text{at}}^{(1)}}{\partial x_{\text{A}}^{(1)}} \approx \mu_{\alpha} + k_B T \ln \frac{c_{\alpha}}{1 - c_{\alpha}}, \quad (22)$$

where the *circa* (\approx) corresponds to approximation (a)²⁹.

Equation (17) can be solved with respect to c_{α} with the help of Eqs. (21,22) as

$$c_{\alpha} = \left[1 + \exp \frac{E_{\text{sol}}^{\alpha}(A)}{k_B T} \right]^{-1} \simeq \exp \left(- \frac{E_{\text{sol}}^{\alpha}(A)}{k_B T} \right) \Big|_{k_B T \ll E_{\text{sol}}^{\alpha}(A)}, \quad (23)$$

where

$$\begin{aligned} E_{\text{sol}}^{\alpha}(A) &= \mu_{\alpha} - \frac{\partial E_{\text{at}}^{\text{mix}}}{\partial x_{\text{A}}^{\text{gen}}} \\ &= \frac{1}{x_{\text{A}}^{\text{gen}}} \left[E_{\text{at}}^{(1)} + \mu_{\alpha} x_{\text{A}}^{\text{gen}} - \left(E_{\text{at}}^{(1)} + \frac{\partial E_{\text{at}}^{\text{mix}}}{\partial x_{\text{A}}^{\text{gen}}} x_{\text{A}}^{\text{gen}} \right) \right] \\ &= \frac{1}{x_{\text{A}}^{\text{gen}}} \left[E_{\text{at}}^{(1)}(x^{\text{gen}}) - E_{\text{at}}^{\text{mix}}(x^{\text{gen}}) \right]. \end{aligned} \quad (24)$$

Both Equations (24) and (3) define the same quantity: the low-solubility formation energy, $E_{\text{sol}}^{\alpha}(A)$, determining the low-solubility of *A*-solute in α type positions. In addition, by using Eqs. (8)-(23)²⁹ the total equilibrium concentration of solute *A* in the phase (1) becomes

$$x_{\text{A}}^{(1)} \approx \frac{\nu c_{\alpha}}{n_{\text{uc}} + m_{\text{uc}}}, \quad (25)$$

where c_{α} is determined by Eq. (23).

Approximation (b) can be relaxed if the various types of substitutional and interstitial positions are occupied independently. This is expected to be true in the low solute concentration limit. Thus, expression (25) can be integrated out through the various types of positions, leading to

$$x_{\text{A}}^{(1)} \approx \frac{\sum_i \nu_i c_i + \sum_s \nu_s c_s}{n_{\text{uc}} + m_{\text{uc}}}, \quad (26)$$

where c_i and c_s are obtained from a set of Eq. (23), by using the corresponding $E_{\text{sol}}^{(i)}(A)$ and $E_{\text{sol}}^{(s)}(A)$ for each type of defects.

VI. FIRST-PRINCIPLES CALCULATIONS

The first-principles calculations of energies are performed by using our high-throughput quantum calculations framework AFLOW^{20,30,31,32} and the software VASP³³. We use projector augmented waves (PAW) pseudopotentials³⁴ and exchange-correlation functionals as parameterized by Perdew and Wang³⁵ for the generalized gradient approximation (GGA). Simulations are carried out without spin polarization (not required for the elements under investigation), at zero temperature, and without zero-point motion. All structures are fully relaxed (shape and volume of the cell and internal positions of the atoms). The effect of lattice vibrations is omitted. Numerical convergence to within about 1 meV/atom is ensured by enforcing a high energy cut-off (414 eV) and dense 4,500 **k**-point meshes.

Ground states determination

The calculation of solubility of *A* in Mg-B compounds requires the knowledge of the relevant ground states in

the ternary Mg-B-A system. The systems under investigations have not been well characterized experimentally or theoretically, and only the binary Mg-B, B-A, and Mg-A systems have been studied. Hence, we performed additional high-throughput searches to determine if further ground states exist in the three binary systems^{20,30,31,32}. Based on the knowledge of the binary systems, we built³⁶ the ternary ground state phase diagrams for Mg-B-A, with the expectation that no *missed* ternary ground state is relevant to the solubility of A (Ref. 37).

TABLE IV: The formation energies $\Delta E_{\text{at}}^{\text{bin}}$ (Eq. (27)) for Mg-B, B-A, and Mg-A binary ground states ($A=\text{Li, Be, Na, Mg, K, Ca, Rb, Sr, Cs, Ba}$). The symbol (+) indicates possible ground states never observed experimentally (CaB₄ and RbB₄). The symbol (-) indicates the experimentally observed Sr₉Mg₃₈, which was not confirmed to be a ground states by first-principle calculations.

	$\Delta E_{\text{at}}^{\text{bin}}$ (eV/at.)	Proto- type ¹⁹	Space group ³⁸	Pearson	Ref.
Li ₃ B ₁₄	-0.219	Li ₃ B ₁₄	I42d(122)	tI160	39
LiB ₃	-0.235	LiB ₃	P4/mbm(127)	tP20	40
Li ₈ B ₇	-0.216	Li ₈ B ₇	P6m2(187)	hP15	32
Be ₃ B ₅₀	-0.032	Be ₃ B ₅₀	P4 ₂ /nm(134)	tP53	41
Be _{1.11} B ₃	-0.096	Be _{1.11} B ₃	P6/mmm(191)	hP111	42
MgBe ₁₃	-0.009	NaZn ₁₃	Fm3c(226)	cF112	43
NaB ₁₅	-0.059	NaB ₁₅	Imma(74)	oI64	44
Na ₃ B ₂₀	-0.070	Na ₃ B ₂₀	Cmmm(65)	oC46	45
MgB ₇	-0.138	MgB ₇	Imma(74)	oI64	46
MgB ₄	-0.152	MgB ₄	Pnma(62)	oP20	47
MgB ₂	-0.151	AlB ₂	P6/mmm(191)	hP3	48
KB ₆	-0.043	CaB ₆	Pm3m(221)	cP7	49
CaB ₆	-0.423	CaB ₆	Pm3m(221)	cP7	50
CaB ₄ (+)	-0.410	UB ₄	P4/mbm(127)	tP20	51
CaMg ₂	-0.128	MgZn ₂	P6 ₃ /mmc(194)	hP12	52
RbB ₄ (+)	-0.163	UB ₄	P4/mbm(127)	tP20	-
SrB ₆	-0.464	CaB ₆	Pm3m(221)	cP7	53
Sr ₂ Mg ₁₇	-0.055	Th ₂ Ni ₁₇	P6 ₃ /mmc(194)	hP38	54
Sr ₉ Mg ₃₈ (-)	-0.070	Sr ₉ Mg ₃₈	P6 ₃ /mmc(194)	hP94	55
Sr ₆ Mg ₂₃	-0.085	Th ₆ Mg ₂₃	Fm3m(225)	cF116	56
SrMg ₂	-0.114	MgZn ₂	P6 ₃ /mmc(194)	hP12	57
BaB ₆	-0.421	CaB ₆	Pm3m(221)	cP7	53
Ba ₂ Mg ₁₇	-0.072	Zn ₁₇ Th ₂	R3mh(166)	hR57	54
Ba ₆ Mg ₂₃	-0.085	Th ₆ Mg ₂₃	Fm3m(225)	cF116	56
BaMg ₂	-0.097	MgZn ₂	P6 ₃ /mmc(194)	hP12	57

The existence of the ground states for a given binary A - B system is based on binary *bulk* formation energy, which, for each phase ϕ with stoichiometry $A_{x_A}B_{x_B}$, is determined with respect to pure A and B energies $E_{\text{at}}(A)$ and $E_{\text{at}}(B)$ as

$$\Delta E_{\text{at}}^{\text{bin}}(\phi) \equiv E_{\text{at}}(\phi) - x_A E_{\text{at}}(A) - x_B E_{\text{at}}(B). \quad (27)$$

The results are presented at Table IV and in Figure 1. For each element A , the reference energy is chosen to be the lowest among the pure fcc, bcc and hcp energies⁵⁸. The reference energy for boron is taken to be α -boron (Refs. 19,31,59,60,61).

All experimentally observed phases are confirmed except for Sr₉Mg₃₈ (P6₃/mmc). We also find two possible

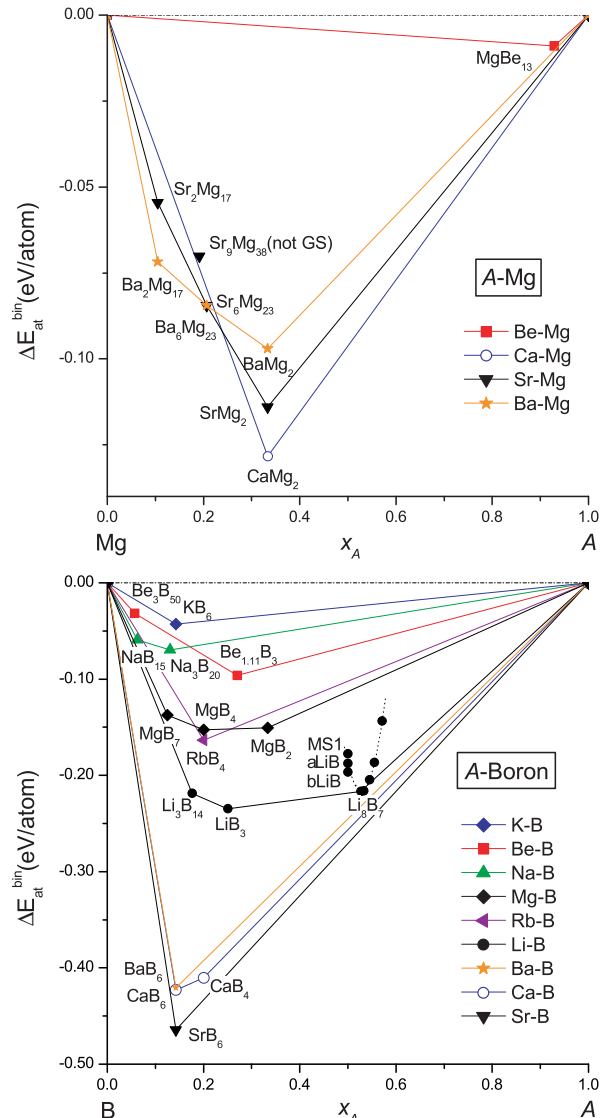


FIG. 1: (Color online) Formation energies $\Delta E_{\text{at}}^{\text{bin}}$ for Mg-B, B-A, and Mg-A binary ground states ($A=\text{Li, Be, Na, Mg, K, Ca, Rb, Sr, Cs, Ba}$) from Table IV. The dashed parabola for the Li-B system indicates the linear chains phases of Ref. 32

new phases, CaB₄ and RbB₄, both P4/mbm (#127) and with UB₄ prototype (CaB₄ was previously identified in *ab initio* online database⁵¹). The formation energies for Ba₂Mg₁₇, Ba₆Mg₂₃, BaMg₂, and CaMg₂ are similar to those of Ref. 62 (reported as -0.079 eV, -0.089 eV, -0.088 eV, and -0.126 eV, respectively). The small differences can be explained on the basis of different GGA pseudopotentials (PW91 versus PBE) and different energy cut-offs (414 eV versus 360 eV). Our results can not be compared with the thermodynamic discussion based on the semi-empirical Miedema method reported in Ref. 14, because

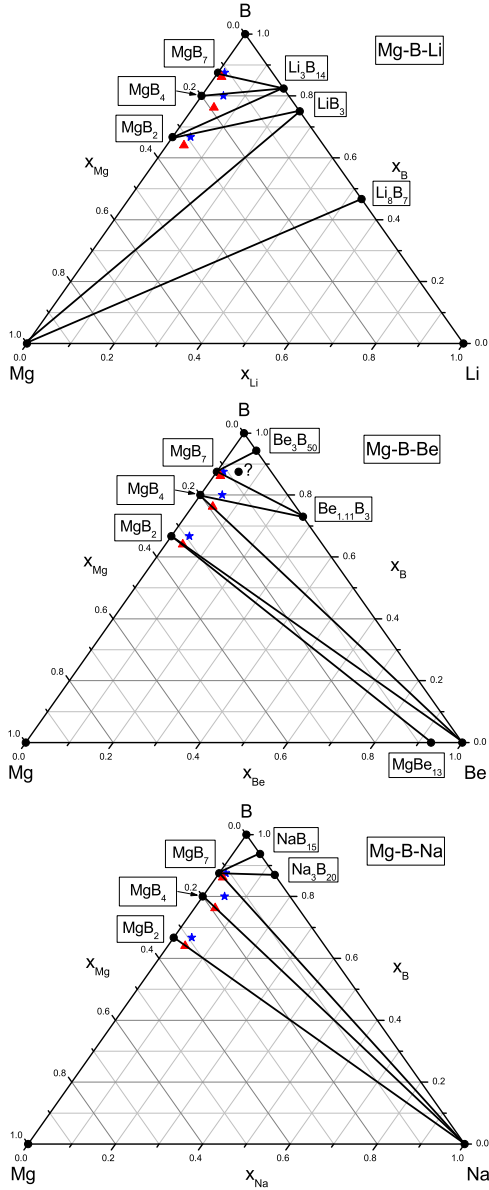


FIG. 2: (color online) The ternary ground state phase diagrams of Mg-B-A alloys ($A=\text{Li, Be, Na}$). The filled circles represent known ground states. The blue stars and red triangles represent the substitutional ($\text{Mg}_7\text{B}_{56}A$, $\text{Mg}_3\text{B}_{16}A$, $\text{Mg}_7\text{B}_{16}A$) and interstitial ($\text{Mg}_8\text{B}_{56}A$, $\text{Mg}_4\text{B}_{16}A$, $\text{Mg}_8\text{B}_{16}A$) supercells, respectively. Each supercell has been constructed from the most appropriate Mg-B compound (MgB_2 , MgB_4 , or MgB_7). The question mark in the Mg-B-Be system indicates the existence of new possible ternary ground state(s) (Sec. VI).

we include further ground state prototypes other than those used in the heat of formations fitting in Ref. 14.

The calculated ternary ground state phase diagrams for Mg-B-A alloys are depicted in Figs. 2,3,4. Note that in each phase diagram, the red triangles and blue stars

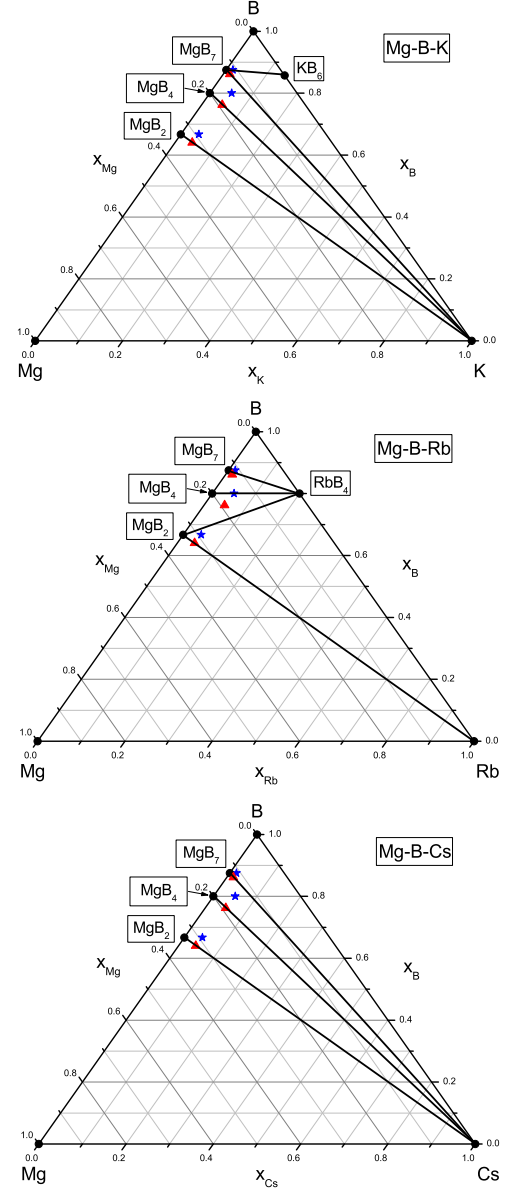


FIG. 3: (color online) The ternary ground state phase diagrams of Mg-B-A alloys ($A=\text{K, Rb, Cs}$).

represent the supercells with one interstitial or substitutional A atom, respectively. In the interstitial case, the supercells belong to the lines $\text{Mg}_n\text{B}_m \leftrightarrow A$, while in the substitutional case, the supercells belong to the lines parallel to $\text{Mg} \leftrightarrow A$ and intersecting the Mg_nB_m (constant B concentration).

Formation energies numerical results

The calculated parameters of the model (“raw” μ_i , $\bar{\mu}_s$ (Eq. (1)), “true”- $E_A^{(i)}$, $E_A^{(s)}$ (Eq. (2)) and low-solubility $E_{\text{sol}}^{(i)}$, $E_{\text{sol}}^{(s)}$ (Eqs. (3)) formation energies) are presented

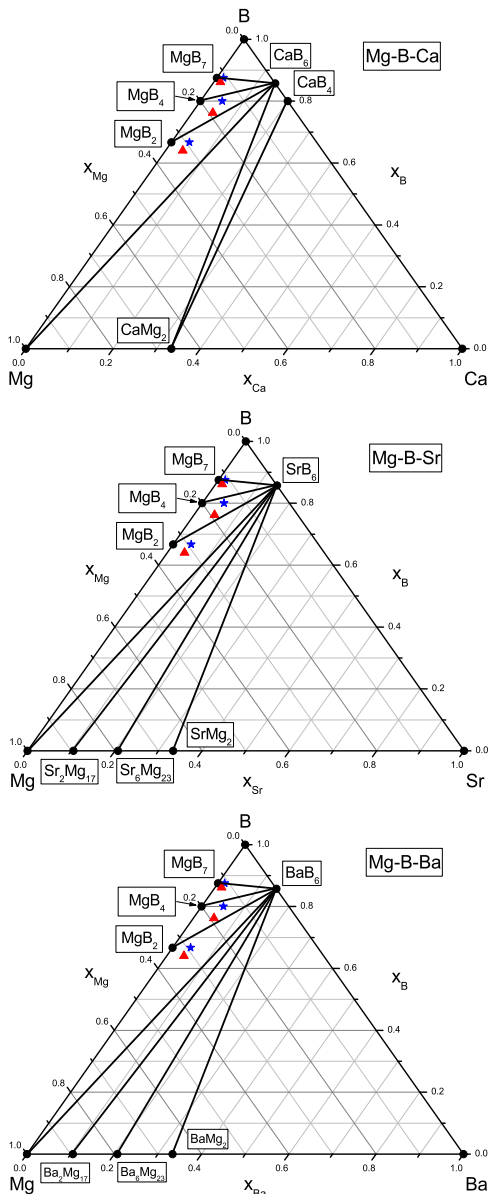


FIG. 4: (color online) The ternary ground state phase diagrams of Mg-B-A alloys ($A=\text{Ca, Sr, Ba}$).

in Table V and in Fig. 5.

The values of the low-solubility energies reported in Table V suggest the following. (a) Only $E_{\text{sol}}^{(s)}$ for substitutional Be in MgB_7 was found to be negative, indicating the existence of unknown ground state(s) within the triangle $\text{MgB}_7 \leftrightarrow \text{Be}_3\text{B}_{50} \leftrightarrow \text{Be}_{1.11}\text{B}_3$. This fact is summarized by the question mark in Fig. 2. (b) Generally, the substitutional systems have lower formation energy than the interstitial systems. Exceptions are Be, Cs, and Ba in MgB_2 ; (c) Although oscillating, the formation energies tends to increase with the element number, as shown in Fig. 5. Regular oscillations are observed

TABLE V: Interstitial (i) and substitutional (s) quantities for alkali and alkaline earth solute elements A in MgB_2 , MgB_4 , and MgB_7 compounds: “raw” formation energies μ_i , $\bar{\mu}_s$ (Eq. (1)), “true” formation energies $E_A^{(i)}$, $E_A^{(s)}$ (Eq. (2)) and low-solubility formation energies $E_{\text{sol}}^{(i)}$, $E_{\text{sol}}^{(s)}$ (Eqs. (3)). In each case, the presented value is the lowest one among all the possible interstitial or substitutional positions.

A	(eV)	MgB_2		MgB_4		MgB_7	
		(i)	(s)	(i)	(s)	(i)	(s)
Li	$\mu_i, \bar{\mu}_s$	0.542	-0.111	0.234	-0.109	-0.959	-0.055
	$E_A^{(i,s)}$	2.444	0.310	2.136	0.312	0.943	0.366
	$E_{\text{sol}}^{(i,s)}$	2.716	0.574	2.654	0.686	1.657	0.506
Be	$\mu_i, \bar{\mu}_s$	-2.665	-0.876	-0.506	-0.710	-1.577	-2.100
	$E_A^{(i,s)}$	1.042	1.350	3.201	1.516	2.130	0.126
	$E_{\text{sol}}^{(i,s)}$	1.054	1.21	3.201	1.256	2.181	-0.557
Na	$\mu_i, \bar{\mu}_s$	5.623	1.839	2.409	1.285	1.999	0.869
	$E_A^{(i,s)}$	6.932	1.666	3.718	1.113	3.308	0.697
	$E_{\text{sol}}^{(i,s)}$	6.944	1.526	3.718	0.802	3.308	0.147
K	$\mu_i, \bar{\mu}_s$	7.022	4.674	2.984	3.001	3.453	2.077
	$E_A^{(i,s)}$	8.061	4.232	4.023	2.559	4.492	1.635
	$E_{\text{sol}}^{(i,s)}$	8.073	4.092	4.023	2.248	4.492	0.838
Ca	$\mu_i, \bar{\mu}_s$	2.833	-0.295	1.042	-1.107	1.251	-1.941
	$E_A^{(i,s)}$	4.751	-0.732	2.960	-0.671	3.169	-1.504
	$E_{\text{sol}}^{(i,s)}$	6.364	1.747	4.993	1.218	5.453	0.358
Rb	$\mu_i, \bar{\mu}_s$	9.463	6.572	3.733	3.957	4.751	3.312
	$E_A^{(i,s)}$	10.393	6.021	4.663	3.406	5.681	2.761
	$E_{\text{sol}}^{(i,s)}$	10.406	5.981	4.862	3.460	6.047	2.477
Sr	$\mu_i, \bar{\mu}_s$	5.514	1.761	1.334	0.221	2.149	-0.960
	$E_A^{(i,s)}$	7.138	1.618	2.958	0.364	3.773	-0.817
	$E_{\text{sol}}^{(i,s)}$	9.042	3.802	5.282	2.544	6.348	1.331
Cs	$\mu_i, \bar{\mu}_s$	4.663	8.436	4.559	5.064	6.488	5.131
	$E_A^{(i,s)}$	5.523	7.815	5.419	4.444	7.349	4.510
	$E_{\text{sol}}^{(i,s)}$	5.536	7.675	5.419	4.134	7.349	3.411
Ba	$\mu_i, \bar{\mu}_s$	2.450	3.959	1.365	1.084	3.118	0.335
	$E_A^{(i,s)}$	4.373	3.518	3.288	1.525	5.041	0.777
	$E_{\text{sol}}^{(i,s)}$	5.971	5.99	5.306	3.400	7.309	2.624

for all substitutional systems starting with Na. The lower and higher boundaries of such correspond to alkaline earth and alkali elements, respectively. (d) Na, Ca, and Li substitutionals in MgB_7 have the lowest formation energies (0.147 eV, 0.358 eV, and 0.506 eV, respectively), resulting in high solubility (Sec. VII). (e) In general for substitutional systems, the higher boron contents the lower formation energy (except Li and Be). (f) The corresponding “true” $E_A^{(i,s)}$ and low-solubility $E_{\text{sol}}^{(i,s)}$ (A) formation energies generally demonstrate a similar behavior as functions of A . Exceptions are $E_A^{(s)} < 0$ for $A=\text{Ca}$ and Sr and $E_{\text{sol}}^{(i,s)}(A) < 0$ for $A=\text{Be}$. The difference is due to the consideration of all the known ground states for the determination of $E_{\text{sol}}^{(i,s)}$ and not only pure Mg, B and A (as for $E_A^{(i,s)}$).

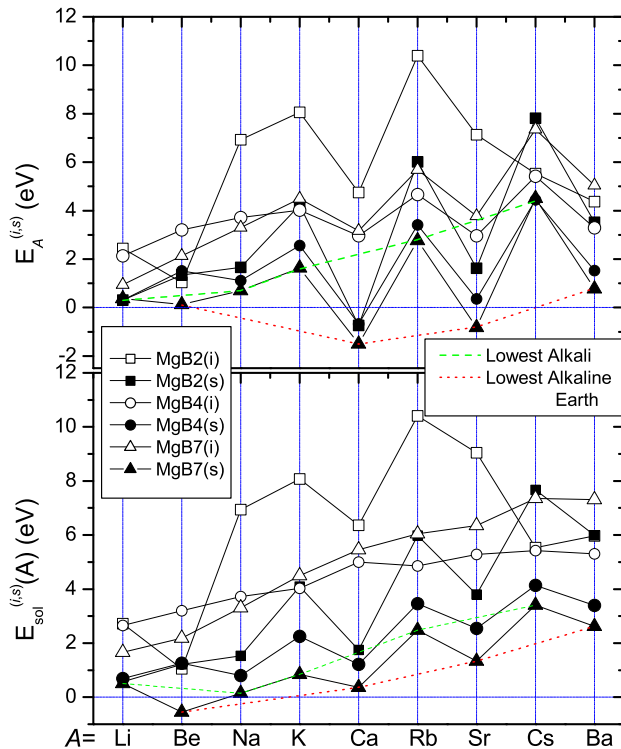


FIG. 5: (Color online) Representation of the formations energies from Table V. Dashed (green) and dotted (red) lines connect the lowest formation energies for alkali and alkaline earth elements, respectively.

For Li-Mg-B, in Ref. 17 the formation energies were obtained from first principles for interstitial and substitutional Li in boron-rich MgB_2 (3.00 eV and 0.27 eV, respectively). The results of Ref. 17 are different from our low-solubility formation energies $E_{\text{sol}}^{(i)}(\text{Li})=2.72$ eV and $E_{\text{sol}}^{(s)}(\text{Li})=0.57$ eV (see Table V), because only the hexagonal α -LiB phase was considered as a ground state in Ref. 17 and the other boron-rich phases were reported to be unstable (the α -LiB was refined in Ref. 32 by variational minimization of the Li and B concentration as Li_8B_7). However, in our high-throughput framework, we found LiB_3 and Li_3B_{14} to be stable⁶³, and the appropriate analysis of the formation energies should be done with respect to the triangle $\text{MgB}_2 \leftrightarrow \text{LiB}_3 \leftrightarrow \text{Mg}$ as shown in Fig. 2. In the low-solubility limit of Li, since the supercell concentration is close to MgB_2 , the lever rule of phase decomposition of the mixtures does not cause significant errors if the energies are calculated with respect to other references, and therefore the results of Ref. 17 are somehow similar.

For Na-Mg-B, it can be shown that the substitutional Na formation energy in magnesium-rich MgB_2 (1.74 eV) obtained in Ref. 17 is equivalent to our “true” formation

energy for substitutional Na in MgB_2 ($E_{\text{Na}}^{(s)} = 1.67$ eV, see Table V). The observed small numerical difference between two results can be attributed to the different energy cutoffs for the basis set (414 eV versus 312 eV)⁶⁴.

VII. SOLUBILITY RESULTS

Solubility results are presented in Table VI (the low-solubility approximation values are shown in brackets). We report only values larger than 10^{-6} (Li, Na, Ca, and K). The values on Table VI suggest the following. (a) Na is the only element which has a substantial solubility: Na in MgB_7 is $\sim 0.5\text{-}1\%$ at $T = 650 - 1000$ K. (b) The substitutional solubility of Be in MgB_7 can not be determined because the corresponding formation energy $E_{\text{sol}}^{(s)}$ (see Eq. (3)) is negative implying that the ground state list is not complete. Thus the approach of Sec. V is not applicable. (c) In agreement with their lowest formation energies $E_{\text{sol}}^{(s)}$ (Table V and Fig. 5), substitutional Li, Na, and Ca experience the largest solubilities among all studied systems; (d) Due to their considerably high formation energies $E_{\text{sol}}^{(i)}$ (Table V and Fig. 5), all the investigated interstitial systems have negligible solubilities. (e) The low-solubility approximation and the general theory agree within 5%.

The calculated negligible solubilities of Be, Na, Ca in MgB_2 agree with previous experimental observations^{4,7,8,11,12,13}. We did not find any sign of nonvanishing solubilities of Rb, Cs and Ba in the MgB_2 alloy even at high annealing temperature in disagreement with the reported experimental data of Ref. 9. However, our negligible Rb and Cs solubility in bulk MgB_2 are in agreement with the experimental conclusion made in Ref. 10 where the author suggest that Rb and Cs dopants most likely segregate in grain boundaries.

The obtained low solubilities of Li and Sr in MgB_2 differ from experimental values (solubility up to 30% in Refs. 2,3,4,5,6,13). This discrepancy can be attributed to segregation of Li and Sr in the grain boundaries as was concluded for Rb and Cs in Ref. 10. In particular, the value of $E_{\text{sol}}^{(s)}=3.8$ eV for Sr is too large for non-negligible bulk solubility. For Li in MgB_2 the calculated formation energy $E_{\text{sol}}^{(s)}=0.57$ eV is not very large and it is the smallest among the investigated solutes in MgB_2 . In Ref. 17, qualitative conclusions about high solubility of Li and low solubility of Na in MgB_2 were made based on a large difference between the corresponding formation energies. Our numerical results demonstrate that, despite much lower formation energy of Li in comparison with Na in MgB_2 , the Li-solubility is still very low (Sec. VI).

It should be emphasized that our model is in thermodynamical equilibrium which can be difficult to reach at

TABLE VI: Calculated equilibrium interstitial $x_{\text{A}(i)}^{(1)}$ (i) and substitutional $x_{\text{A}(s)}^{(1)}$ (s) A-solute concentrations at temperatures $T = 300, 650,$ and 1000 K, in $\text{MgB}_2, \text{MgB}_4,$ and MgB_7 compounds. The values obtained within the low-solubility approximation are reported in brackets. Zeros are used for values smaller than 10^{-6} . For Be “ $\Delta E < 0$ ” indicates that the corresponding formation energy $E_{\text{so1}}^{(s)}$ (see Eq. (3)) is negative implying that the ground state(s) list is not complete and the approach of Sec. V is not applicable.

A	T (K)	$x_{\text{A}(i,s)}^{(1)}$		MgB_2		MgB_4		MgB_7	
		i	s	i	s	i	s	i	s
Li	300	0	0	0	0	0	0	0	0
	650	0	1.3×10^{-5} (1.2×10^{-5})	0	0	0	0	0	9.9×10^{-6} (9.9×10^{-6})
	1000	0	4.5×10^{-4} (4.3×10^{-4})	0	6.9×10^{-5} (7.0×10^{-5})	0	0	0	2.6×10^{-4} (2.6×10^{-4})
Be	300	0	0	0	0	0	0	0	$\Delta E < 0$
	650	0	0	0	0	0	0	0	$\Delta E < 0$
	1000	0	0	0	0	0	0	0	$\Delta E < 0$
Na	300	0	0	0	0	0	0	0	2.1×10^{-4} (2.1×10^{-4})
	650	0	0	0	0	0	0	0	4.4×10^{-3} (4.2×10^{-3})
	1000	0	0	0	1.8×10^{-5} (1.8×10^{-5})	0	0	0	1.0×10^{-2} (0.96×10^{-2})
K	300	0	0	0	0	0	0	0	0
	650	0	0	0	0	0	0	0	0
	1000	0	0	0	0	0	0	0	3.6×10^{-6}
Ca	300	0	0	0	0	0	0	0	0
	650	0	0	0	0	0	0	0	1.1×10^{-4} (1.0×10^{-4})
	1000	0	0	0	0	0	0	0	1.0×10^{-3} (0.96×10^{-3})
Rb	300	0	0	0	0	0	0	0	0
	650	0	0	0	0	0	0	0	0
	1000	0	0	0	0	0	0	0	0
Sr	300	0	0	0	0	0	0	0	0
	650	0	0	0	0	0	0	0	0
	1000	0	0	0	0	0	0	0	0
Cs	300	0	0	0	0	0	0	0	0
	650	0	0	0	0	0	0	0	0
	1000	0	0	0	0	0	0	0	0
Ba	300	0	0	0	0	0	0	0	0
	650	0	0	0	0	0	0	0	0
	1000	0	0	0	0	0	0	0	0

low temperatures and the experimental equilibrium solubility tends usually to be overestimated. In fact, the formation of metastable and/or unstable states which are subsequently frozen at low temperatures, can make solubility measurements very challenging. In such scenarios, the measured solubility may correspond to spinodal concentration rather than actual binodal concentration or simply characterize the frozen out of equilibrium solubility remaining from the initial specimen preparation at higher temperature. Besides, the segregation of defects

into grain-boundaries, especially in multicrystalline samples prepared through non optimal cooling dramatically affect the amount of frozen defects and solutes.

Although in our study we did not perform an extensive search over the configurational space of ternary alloy, if a new ternary phases were present near MgB_2 , the solute atoms would concentrate and nucleate such phases, and this may be misinterpreted as a high solubility in MgB_2 phase. Furthermore, a new equilibrium ternary phase would result in an increase of impurities formation energies and, correspondingly, in a decrease of solubility. Numerical approximations in the first-principles are not expected to affect the values of solubility: i.e. typically for $\delta E_{\text{so1}} \sim 30$ meV/atom, $\delta x_{\text{A}}^{(1)} \sim 2 \times 10^{-4}$. Lattice vibrations and solute-solute interactions are neglected because they are not expected to play important roles at low temperatures and low solute concentrations.

VIII. CONCLUSIONS

In the present paper, we present an approach to study the solubilities in ternary alloys. The advantage of the approach is in taking into account all known ternary ground states rather than just pure solids. Based on the approach, we propose an analytical low-solubility approximation that can be used for high-throughput calculations of solubilities in alloys.

Combining the developed approach with first principle calculations, we have determined the formation energies and solubilities of alkali (Li, Na, K, Rb, Cs) and alkaline earth (Be, Ca, Sr, Ba) metals in the Mg-B system. It is found that the considered metals have low solubilities in the boron-rich Mg-B alloy. Substitutional Na, Ca, and Li experience the the largest solubilities, with Na in MgB_7 reaching 0.5-1% at $T = 650 - 1000$ K. All the considered interstitial scenarios lead to negligible solubilities. The solubility of Be in MgB_7 can not be determined with our model because the corresponding low-solubility formation energy is negative implying that the existing ground states list must be augmented through a more extensive search over the configurational space.

We also present a high-throughput search of ground states in binary Mg-B, Mg-A, and B-A alloys ($A = \text{Li, Be, Na, Mg, K, Ca, Rb, Sr, Cs, Ba}$). Ternary phase diagrams Mg-B-A are constructed based on of the determined phases. $\text{Sr}_9\text{Mg}_{38}$ is not an equilibrium ground state despite its high temperature validations. Two new ground states CaB_4 and RbB_4 are found.

Acknowledgements

We acknowledge Mike Mehl, Igor Mazin, and Wahyu Setyawan for fruitful discussions. This research was sup-

ported by ONR (Grants No. N00014-07-1-0878 and N00014-07-1-1085) and NSF (Grant No. DMR-0639822) We thank the Teragrid Partnership (Texas Advanced

Computing Center, TACC) for computational support (MCA-07S005).

-
- * Electronic address: stefano@duke.edu
- ¹ J. Nagamatsu, N. Nakagawa, T. Muranaka, Y. Zenitani, and J. Akimitsu, *Nature* (London) **410**, 63 (2001).
 - ² F. J. Owens, *Physica C* **363**, 202 (2001).
 - ³ Y. G. Zhao, X. P. Zhang, P. T. Qiao, H. T. Zhang, S. L. Jia, B. S. Cao, M. H. Zhu, Z. H. Han, X. L. Wang, and B. L. Gu, *Physica C* **361**, 91 (2001).
 - ⁴ X. P. Zhang, Y. G. Zhao, P. T. Qiao, Z. S. Yin, S. L. Jia, B. S. Cao, M. H. Zhu, Z. H. Han, Y. H. Xiong, P. J. Li, and B. L. Gu, *Journal of Superconductivity: Incorporating Novel Magnetism*, **15**, 159 (2002).
 - ⁵ M. R. Cimberle, M. Novak, P. Manfrinetti, and A. Palenzona, *Supercond. Sci. Technol.* **15**, 47 (2002).
 - ⁶ J. Karpinski, N. D. Zhigadlo, S. Katrych, K. Rogacki, B. Batlogg, M. Tortello, and R. Puzniak, *Phys. Rev. B* **77**, 214507 (2008).
 - ⁷ P. Toulemonde, N. Musolino, H. L. Suo, and R. Flükiger *Journal of Superconductivity: Incorporating Novel Magnetism* **15**, 613 (2002).
 - ⁸ A. Agostino, M. Panetta, P. Volpe, M. Truccato, S. Cagliero, L. Gozzelino, R. Gerbaldo, G. Ghigo, F. Laviano, G. Lopardo, and B. Minetti, *IEEE Transactions on Applied Superconductivity* **17**, 2774 (2007).
 - ⁹ A. V. Palmichenko, O. M. Vyaselev and N. S. Sidorov, *JETP Letters* **86**, 272 (2007).
 - ¹⁰ R. K. Singh, Y. Shen, R. Gandikota, D. Wright, C. Carvalho, J. M. Rowell, and N. Newman, *Supercond. Sci. Technol.* **21**, 025012 (2008).
 - ¹¹ I. Felner, *Physica C* **353**, 11 (2001).
 - ¹² C. H. Cheng, Y. Zhao, X. T. Zhu, J. Nowotny, C. C. Sorrell, T. Finlayson, and H. Zhang, *Physica C* **386**, 588 (2003).
 - ¹³ A. Tampieri, G. Celotti, S. Sprio, and D. Rinaldi, *International Journal of Modern Physics B* **17**, 438 (2003).
 - ¹⁴ X. S. Wu and J. Gao, *Physica C* **418**, 151 (2005).
 - ¹⁵ A. R. Miedema, P. F. de Chatel, F. R. de Boer, *Physica B & C* **100**, 1 (1980).
 - ¹⁶ W. Toop, *Trans. Met.* **237**, 738 (1965).
 - ¹⁷ F. Bernardini and S. Massidda, *Europhys. Lett.*, **76**, 491 (2006).
 - ¹⁸ T. B. Massalski, *Binary Alloy Phase Diagrams*, 2nd ed. (ASM International, Materials Park, OH, 2003).
 - ¹⁹ *Pauling file: Inorganic Materials Database and Design System - Binaries Edition*, edited by P. Villars (ASM International, Metals Park, OH, 2002).
 - ²⁰ S. Curtarolo, D. Morgan, and G. Ceder, *Calphad* **29**, 163-211 (2005).
 - ²¹ S. Curtarolo, *Aflow: a computational software to calculate properties of materials in a high-throughput fashion*. <http://materials.pratt.duke.edu/afLOW.html>
 - ²² Y. Mishin and D. Farkas, *Phil. Mag. A* **75**, 169 (1997); Y. Mishin and C. Herzig, *Acta Mater.* **48**, 589 (2000).
 - ²³ The bar at $\bar{\mu}_s$ indicates that the quantity is not a chemical potential itself, as the number of particle is conserved.
 - ²⁴ R. V. Chepulskii and S. Curtarolo, "Calculation of solubility in titanium alloys from first-principles", submitted to *Acta Materialia* (2009). <http://arxiv.org/abs/0901.0200>
 - ²⁵ M. A. Krivoglaz and A. A. Smirnov, *The Theory of Order-Disorder in Alloys* (Macdonald, London, 1964).
 - ²⁶ C. Wagner and W. Schottky, *Z. Physik. Chem. B* **11**, 163 (1930).
 - ²⁷ In this method, the general composition x^{gen} plays just a supplementary role not effecting the results if x^{gen} necessarily belongs to the three-phase compositional triangle.
 - ²⁸ C. Sigli, L. Maenner, C. Sztur, and R. Shahni, in *Proceedings of the 6th International Conference on Aluminum Alloys (ICAA-6)*, edited by T. Sato et al. (Japan Institute of Light Metals, 1998), Vol. 1, p. 87
 - ²⁹ In this case, the approximation (a) implies the neglect of $x_{\text{A}^{(i)}}^{(1)}$ in Eq. (15) and c_i in the denominator of Eq. (10), respectively.
 - ³⁰ S. Curtarolo, D. Morgan, K. Persson, J. Rodgers, and G. Ceder, *Phys. Rev. Lett.* **91**, 135503 (2003).
 - ³¹ A. N. Kolmogorov and S. Curtarolo, *Phys. Rev. B* **73**, 180501(R) (2006).
 - ³² A. N. Kolmogorov and S. Curtarolo, *Phys. Rev. B* **74**, 224507 (2006).
 - ³³ G. Kresse and J. Hafner, *Phys. Rev. B* **47**, 558 (1993).
 - ³⁴ P. E. Blochl, *Phys. Rev. B* **50**, 17953 (1994).
 - ³⁵ Y. Wang and J. P. Perdew, *Phys. Rev. B* **44**, 13 298 (1991).
 - ³⁶ <http://www.qhull.org/>
 - ³⁷ The approximation implies that a true-ternary ground state does not exist or, if it exist, it is in a region of the phase diagram not relevant for solubility of A in MgB₂, MgB₄ and MgB₇.
 - ³⁸ *International Tables for Crystallography*, Vol. A, edited by T. Hahn (D. Reidel, Dordrecht, 1983).
 - ³⁹ G. Mair, R. Nesper, and H.G. von Schnering, *Journal of Solid State Chemistry* **75**, 30 (1988).
 - ⁴⁰ G. Mair, H.G. von Schnering, M. Wörle, and R. Nesper, *Zeitschrift für Anorganische und Allgemeine Chemie* **625**, 1207 (1999).
 - ⁴¹ F. X. Zhang, F. F. Xu, and T. Tanaka, *Journal of Solid State Chemistry* **177**, 3070 (2004).
 - ⁴² J. Y. Chan, F. R. Fronczek, D. P. Young, J. F. DiTusa, and P. W. Adams, *Journal of Solid State Chemistry* **163**, 385 (2002).
 - ⁴³ T. W. Baker, *Acta Crystallographica* **15**, 175 (1962).
 - ⁴⁴ R. Naslain and J. S. Kasper, *Journal of Solid State Chemistry* **1**, **150** (1970).
 - ⁴⁵ B. Albert and K. Hofmann, *Zeitschrift für Anorganische und Allgemeine Chemie* **625**, 709 (1999).
 - ⁴⁶ A. Guette, M. Barret, R. Naslain, P. Hagenmuller, L. E. Tergenius, and T. Lundström, *Journal of the Less-Common Metals* **82**, 325 (1981).
 - ⁴⁷ A. Guette, R. Naslain, and J. Galy, *Comptes Rendus Hebdomadaires des Seances de l'Academie des Sciences, Serie*

- C: Sciences Chimiques **275**, 41 (1972).
- ⁴⁸ N. V. Vekshina, L. Y. Markovskii, Y. D. Kondrashev, and T. K. Voevodskaya, Journal of Applied Chemistry of the USSR, translated from Zhurnal Prikladnoi Khimii **44**, 970 (1971).
- ⁴⁹ R. Naslain and J. Etourneau, Comptes Rendus Hebdomadaires des Seances de l'Academie des Sciences, Serie C: Sciences Chimiques **263**, 484 (1966).
- ⁵⁰ L. Pauling and S. Weinbaum, Zeitschrift für Kristallographie, Kristallgeometrie, Kristallphysik, Kristallchemie **87**, 181 (1934).
- ⁵¹ M. Widom *et. al.*, *Alloy Database*, <http://alloy.phys.cmu.edu/>.
- ⁵² H. Nowotny, Zeitschrift für Metallkunde **37**, 31 (1946).
- ⁵³ P. P. Blum and F. Bertaut, Acta Crystallographica **7**, 81 (1954).
- ⁵⁴ E. I. Gladyshevskii, P. I. Kripyakevich, M. Y. Teslyuk, O. S. Zarechnyuk, and Yu. B. Kuz'ma, Soviet Physics Crystallography, translated from Kristallografiya **6**, 207 (1961).
- ⁵⁵ F. E. Wang, F. A. Kanda, C. F. Miskell, and A. J. King, Acta Crystallographica **18**, 24 (1965).
- ⁵⁶ E. I. Gladyshevskii, P. I. Kripyakevich, Yu. B. Kuz'ma, and M. Y. Teslyuk, Soviet Physics Crystallography, translated from Kristallografiya **6**, 615 (1961).
- ⁵⁷ E. Hellner and F. Laves, Zeitschrift für Kristallographie, Kristallgeometrie, Kristallphysik, Kristallchemie **105**, 134 (1943).
- ⁵⁸ Y. Wang, S. Curtarolo, C. Jiang, R. Arroyave, T. Wang, G. Ceder, L. Q. Chen, and Z. K. Liu, Calphad **28**, 79-90 (2004).
- ⁵⁹ Z. Liu, X. Qu, B. Huang, and Z. Li, J. Alloys Compd. **311**, 256 (2000).
- ⁶⁰ H. Rosner and W. E. Pickett, Phys. Rev. B **67**, 054104 (2003).
- ⁶¹ M. Widom and M. Mihalkovic, Phys. Rev. B **77**, 064113 (2008).
- ⁶² H. Zhang, J. Saal, A. Saengdeejing, Y. Wang, L.-Q. Chen and Z. K. Liu, in *Magnesium Technology 2007*, eds. R. S. Beals, A. A. Luo, N. R. Neelameggham and M. O. Pekguleryuz, Minerals, Metals and Materials Society/AIME, (Warrendale, PA, 2007), p. 345.
- ⁶³ H. B. Borgstedt, and C. Guminsky, J. Phase Equilibria **24**, 572 (2003).
- ⁶⁴ As shown in Sec. V, the low-solubility formation energy $E_{\text{sol}}^{(s)}(\text{Na})=1.53$ eV rather than “true” formation energy $E_{\text{Na}}^{(s)} = 1.67$ is more accurate for corresponding solubility characterization when the system is miscible. The 0.14 eV difference between $E_{\text{Na}}^{(s)}$ and $E_{\text{sol}}^{(s)}(\text{Na})$ suggests that the effect of other ground state (MgB_4 , see Fig. 2) on the formation energy and subsequently on the solubility is not negligible.